Tuning the Morphology and Chiroptical Properties of Discrete Gold Nanorods with Amino Acids

Guangchao Zheng, Zhiyong Bao, Jorge Pérez-Juste, Ruolan Du, Wei Liu, Jiyan Dai, Wei Zhang, Lawrence Yoon Suk Lee*, Kwok-Yin Wong*

Department of Applied Biology and Chemical Technology and the State Key Laboratory of Chirosciences, The Hong Kong Polytechnic University, Hung Hom, Kowloon, Hong Kong, China

KEYWORDS. gold-molecules-gold nanostructures, controllability of plasmonic CD, spatial chirality transfer, circularly polarized luminescence32452

ABSTRACT: The synthesis of discrete nanostructures with a strong, persistent, stable plasmonic circular dichroism (PCD) signal is challenging. We report a seed-mediated growth approach to obtain discrete Au nanorods with high and stable chiroptical responses (c-Au NRs) in the visible to near-IR region. The morphology of the c-Au NRs was governed by the concentration of l- or d-cysteine used. The amino acids encapsulated within the discrete gold nanostructure enhance their PCD signal, attributed to coupling of dipoles of chiral molecules with the near-field induced optical activity at the hot spots inside the c-Au NRs. The stability of the PCD signal and biocompatibility of c-Au NRs was improved by coating with silica or protein corona. Discrete c-Au NR@SiO_2 with Janus or core–shell configurations retained their PCD signal even in organic solvents. A side-by-side assembly of c-Au NRs induced by l-glutathione led to further PCD signal enhancement, with anisotropic g factors as high as 0.048.

Molecular design of nanoplasmonics beyond the topological control has been regarded as a big challenge.[1-4] Especially, the columbic dipole-dipole interaction between plasmonic metal nanoparticles (NPs) and chiral molecules induces unusual circular dichroism (CD) in the vicinity of the surface plasmon resonance (SPR) frequency of metal NPs, which is termed as plasmonic CD (PCD).[5] Tuning the SPR of plasmonic nanomaterials can make CD to realize from UV to visible region, even near-IR region, as it is known that the absorption peak of biomolecules are localized in the UV region. Traditionally, there are two different routes of inducing PCD; 1. Adsorbing chiral molecules on the single metal NPs[6-8]; 2. self-assembly of metal NPs with chiral molecules [9, 10]. In the latter route, chiral molecules are situated on the hot-spots, in which the electromagnetic field (EF) significantly amplifies the PCD signal. The mechanism for molecular chirality inducing PCD is partially due to the induced chiral current on the surface of metal NPs.[11] Meanwhile, SPR reciprocally influence chirality of biomolecules in the UV region by changing the angle between their electric and magnetic dipoles.[6] That is well-known theory for demonstrating the chiroptical systems through Coulomb dipole-dipole interaction between metal NPs and biomolecules.[10] PCD reporters recently have been designed in the form of core-molecules-shell nanostructures, in which enhanced EF in the interior gap largely interacts with dipole of molecules.[12-14] Additionally, the size of gap and metal elements sensitively affect PCD as the extra enhanced EF is relied on the strong coupling between core and shell.[12, 13]

Hot-spot-mediated PCD has already made great achievements. However, those traditional PCD reporters are not stable under harsh conditions and over extended time. As a result, the dipole of chiral molecules hardly jump transfer to nearby achiral molecules/SPR through space.[15, 16] Ostovar Pour *et al.* have demonstrated the chiroptical property of D/L-ribose is transferred to noncovalent dyes in the presence of SPR of Ag.[15] It has been noticed that silica shells block chiral molecules directly contact with plasmonic metal NPs and dyes. Chiral molecules still imprint their chiral information to achiral dyes by way of nanoplasmonics. Zhu *et al.* recently observed induced chiral current in the gold NRs when chiral quantum dots (QDs) localized near the surface of gold NRs, in which chiral QDs were generated by the Coulomb interaction between excitons and dipole of L-glutathione.[17] Dipole of chiral molecules can interact with SPR although they are separated by excitons of semiconductor NPs. They have offered a new and innovate way to design molecular nanoplasmonics.

Herein, we demonstrate a novel synthetic approach to extend LSPR-CD of gold-molecules-gold nanostructures (GMG NSs) to near-IR region, and also investigated circularly polarized luminescence (CPL) of nonchiral dyes near the GMG

NSs. GMG NSs achieved a larger PCD response using discrete and monometallic nanostructure. The durability and stability of PCD reporters get enhanced in the discrete nanostructure since the chiral dipoles are protected in the hot-spots. It leads us to deeply research on the interaction between the dipoles and excitons in complex architectures.

Results and Discussions:

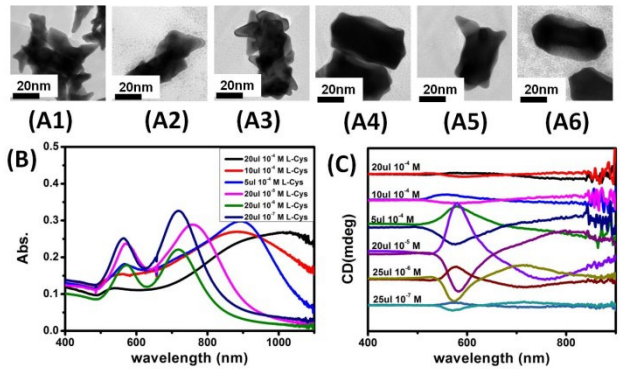

Figure1: (A) TEM images of as-prepared GMG NSs in the different concentration of L-Cys (A1: 20 ul 10^{-4} M; A2: 10 ul 10^{-4} M; A3: 5 ul 10^{-4} M; A4: 20 ul 10^{-5} M; A5: 20 ul 10^{-6} M; A6: 20 ul 10^{-7} M) UV-vis spectra (left) corresponding to CD spectra (middle) and TEM images (right), respectively.

Red-shift SPR of gold nanorods (NRs) to near-IR region (recognized as water window from 800 to 1,200 nm), so far which is one challenge task. If light needs to penetrate deeper in biological tissues, it is necessary to overcome the absorbance by the chromophoroes and water in the visible region. Liz-marzan et al. and many other groups have prepared multi-branched gold nanostars by seed-mediated growth method to red shift SPR of gold nanoparticles (NPs) for biophotonics.[18, 19] Seed-mediated growth approach is one effective approach to synthesize complicated nanostructures, while there are many factors controlling, such as the intrinsic properties of seeds and adatoms (e.g., lattice mismatch), the selectivity of surfactants, and the reaction kinetics.[20-22] We have developed this synthetic technique by using two separated growth stages for overgrowth of gold NRs, which is helpful for us to study the overgrowth mechanism and origin of PCD. UV-vis spectra and Transmission electron microscopy (TEM) image of original gold NRs can be seen in the Figure S1. Gold NRs with LSPR at 730 nm have been obtained by our previous literature, the concentration of gold NRs is estimated around 10^{-9} M. In the first growth stage, the synthesized gold NRs are incubated for 90 min into the solution including few of Au^{3+} (0.1 ml, 1 mM), ascorbic acid (reducing agent: AA, 0.475 mL, 0.1 M), different concentration of L/D Cysteine (L/D-Cys), cetyltrimethylammonium chloride (CTAC) (4 ml, 40 mM). Certain amount of Au^{3+} (0.1 ml, 10 mM) are added in the second growth stage allowing the formation of final GMG NSs and the controllability of PCD.

To clarify the growth and their corresponded chirality mechanism of GMG NSs, we conducted several controlled experiments in the different concentration of L/D-Cys. We noted an optimal range of L/D-Cys concentration for chirality response of GMG NSs. Cyc concentration higher than xx M led to the aggregation of GMG NSs. PCD disappears when the cyc concentration is lower than 20 μL 10^{-7} M since the induced chiral current in GMG NSs has been blocked by its thickness, named shielding effect or screen effect.[23] TEM images from Figure (1, A1) to Figure (1, A6), morphology evolution of GMG NSs from gold nanostars to fat gold NRs as decreasing the concentration of Cys. EDX mapping (Figure S2A to S2C) taken from Sample 1A1 reveals that distribution of Au shells further surface-adsorbed Cys adsorbed between the Au cores and Au shells. The lattice fringes with distance of 0.235 nm were measured by high-resolution TEM images can be designed to the (111) planes of Au (Figure S2D). SAED (inset in figure S2D) suggest that the crystallinity of GMG NSs. At the highest concentration of Cys (above 10^{-4} M), more gold nanospurs are induced on the surface of gold NRs resulting red-shift of LSPR to 1,100 nm. Their LSPR-CD also can extend to the near-IR region but there is limitation of detection in our CD spectrometer beyond 900 nm. As concentration of Cys decreased, size and tips of gold spurs decreased until they disappeared at lowest concentration (around 10^{-7} M). In Figure 1B, LSPR peak of GMG NSs blue-shift and TSPR of peak red-shift when concentration of Cys decreased. PCD of GMG NSs confirm the same shift rules although the intensity of PCD is largest in the middle concentration of Cys in Figure 1C.

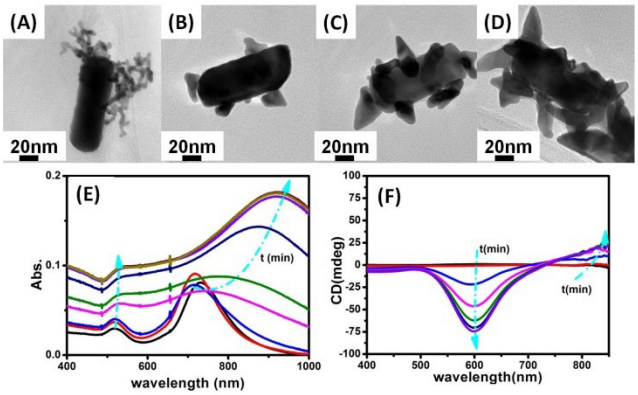

Figure 2 TEM images of growth kinetics of GMG NSs in the presence of 20 ul 10^{-4} M L-Cys in the second growth stage. (A) 0 min; (B) 1 min; (C) 3 min; (D) 15 min. (E) UV-vis and (F) CD spectra of growth kinetics of GMG NSs in the presence of 20 ul 10^{-4} M L-Cys.

Furthermore, we have initially tracked the growth process through TEM, and UV-vis/CD spectroscopy recorded at different growth stages (Figure 2 and Figure S3), which can help us to address the origin of intense chiroplasmonic behavior of GMG NSs and deep clear the growth mechanisms. As shown from Figure 2A to Figure 2D, the second growth stage starts from merging of Au nanodendrites to gold nanospurs, where Au nanodendtrites were formed in the first stage in the presence of 20ul 10^{-4}M of L-Cys. More and larger gold nanospurs are grown at the surface of gold NRs along the growth process. It is confirmed in Figure 2E that red-shift of TSPR absorption with 16 nm (from 520 nm to 536 nm) and red-shift of LSPR absorption with 382 nm (from 718 nm to 1100 nm) due to size of nanospurs increases towards longitudinal direction. Chiral optical behavior has been in-situ monitored through CD spectra in Figure 2F, TSPR-CD with a negative position at 596nm and LSPR-CD

red-shift with a positive value (beyond the limitation of CD spectrometer (200-900 nm)). On the contrary, gold adatoms preferred to grow on the surface of gold NRs along the transverse direction in the concentration of 20 ul 10^{-6} M Cys (Figure S3). There is no nanodentrites formation in the first growth stages (Figure S3A). Transverse size of gold NRs gradually increased although few gold nanospurs are induced at the tips of gold NRs. Therefore, Intensity of TSPR absorbance increased and red-shift from 524 nm to 597 nm as well as the intensity of LSPR increased and red-shift from 708 nm to 751 nm in Figure S3E which is confirmed by the TEM images from Figure S3A to Figure S3D. Intensity of TSPR/LSPR-CD also increased with the time since SPR property is relationship to their size (Figure 3F).

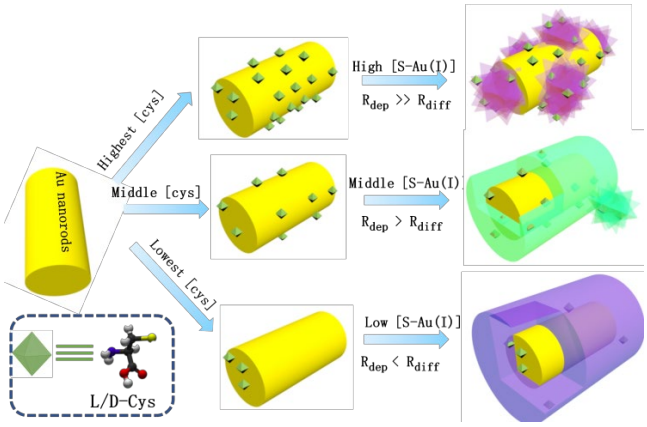

Scheme 1: Synthesis of GMG NSs in the different concentration of L/D-Cys through seed-mediated growth approach.

These characterizations revealed a correlation between the concentration of Cys and the final nanostructure. We have proposed that there are two kinds of Cys in this system including Cys were adsorbed on the surface of gold NRs (surface-adsorbed Cys) and left Cys were distributed into the solution (solution-dispersed Cys). Concentration of surface-adsorbed and solution-dispersed Cys dominates interfacial energy which governs the growth process. (seen Scheme 1) Facets occupied by ligand binding are less exposed and thus decrease the diffusion rate (R_{diff}) to inhibit the growth rate.[24] Previous report revealed that zwitterionic groups can block the longitudinal mode growth and promote the overgrowth along transverse direction due to the Cys preferred to adsorb at the tips of gold NRs.[14] There are two key parameters playing role of growth process, surface-adsorbed Cys through strong chemical bond inhibit R_{diff} of gold adatoms and Thiloate-Au (I) complexes decreasing the deposition rate (R_{dep}) of Au (I) ions by AA since these complexes with lower reduction potentials are much more stable. In the highest concentration of Cys (above 10^{-4}M of Cys), R_{dep} is much larger than R_{diff} while both R_{dep} and R_{diff} are slower. Muti-nanospurs were generated since there are new generated gold nanodentrites in the first growth stage. The gold nanodentrites are merged into gold nanodots which are used as acting catalysts to improve R_{dep} of Au(0) in the second growth stage. In the middle concentration of Cys (from 20 ul 10^{-5} M to 20 ul 10^{-6} M), less Cys occupy the surface of gold NRs leading to R_{diff} increase more than R_{dep}, therefore, gold adatoms grow along the transverse mode as well as less gold nanospurs. Fat nanorods were obtained in the lowest concentration of Cys (at the concentration of 20ul 10^{-7}M), R_{diff} dominates the growth process of Au adatoms resultant Au adatoms only grow along the transverse direction. As a result, intensity of TSPR-CD increased and its position red-shift, meanwhile, position of LSPR-CD blue-shift, when decreasing the concentration of Cys.

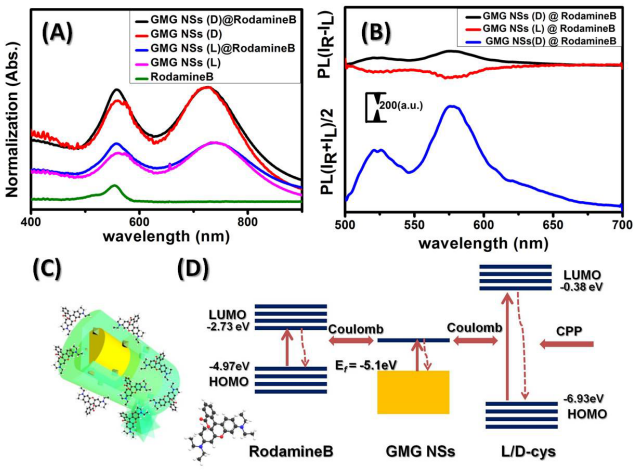

Figure 3 (A) UV-vis spectra of GMG NSs (synthesized in the presence of 20 ul 10^{-5} M Cys) , GMG NSs@Rodamine B, Rodamine B; (B) CPL of GMG NSs@Rodamine B (upper) and CPL of GMG NSs@Rodamine B (bellow) (C) Schematics of a GMG nanostructures functionalzied with Rodamine B. (D) PCD of GMG NSs jump transfer to Rodamine B through coulombic interactions. ***CPP:*** circularly polarized photons.

There are still doubts about the role of surface-adsorbed/ solution-dispersed Cys for the PCD enhancement. Therefore, we firstly set up one experiment so as to remove the excess Cys in the solution after the first growth stage. PCD kept it well maintained the same as no centrifugation in the Figure S4A revealing that surface-adsorbed Cys can imprint their CD to the whole GMG NSs. However, the profile of PCD inversed when D-Cys was added into the second growth solution after centrifugation (Figure S4B), suggesting that solution-dispersed D-Cys endowed their CD to GMG NSs as well as neutralized the PCD resulted from the surface-adsorbed L-Cys. PCD has also been induced without the first growth stage, in which overgrowth process of gold NRs without incubation (Figure S5). It further proves that solution-dispersed Cys can induce the PCD enhancement. Hot-spot mediated exciton-plasmon interaction has been investigated around several orders of magnitude PCD enhancement when chiral molecules localized inside the nanochains.[25] In this manuscript, surface adsorbed-Cys were embedded between the core and shells and solution-dispersed Cys were embedded into the shells which drive PCD enhanced largely upon molecular dipolar field and external SPR fields at the hot-spots.

CPL provides luminescence details upon left-handed and right-handed circularly polarized photons, which breaks the symmetric emission of the excited state of chiral molecular systems. CPL is sensitive to the asymmetric electron transition in the dyes, a CPL spectrum shows us the chiroptical property of transition electron emission state in the

dyes near PCD reporters. Although CPL is quite useful in the sensing, and circularly polarized light sources, research on CPL behavior of chiral nanoplasmonics got few been noticed as traditional PCD reporters are not durable and stable for longer time.[26] Chiral plasmonic systems of Ag NPs capped a dihydrolipoic acid (DHLA) were firstly used to investigate CPL activity by Kumar *et al.* due to their high stability, anisotropy factor and emission quantum yield.[27] The discrete GMG NSs shows certain durability and stability in the strong basic and acidic conditions (Figure S3), which allow us to further study the interaction between dipole of PCD reporters and excitons of achiral dyes. LSPR of GMG NSs functionalization with Rodamine B is a little red-shift and broaden (Figure 3A), and mirror CD spectra still is well maintained although they have a little shift (Figure S7), revealing that Rodamine B localized near the surface of GMG NSs due to LSPR of GMG NSs is sensitive to the dielectric constant of surrounding materials. Figure 3B upper shows mirror polarized luminescence corresponding to the emission spectra of Rodamine B, with two peaks at 576 nm and at 525 nm for the GMG NSs functionalized Rodamine B. PCD destroyed symmetric emission states of Rodamine B via coulomb interactions of plasmon-excitons. Chirality in the L/D-Cys most indirectly responsible for chiroptical property in emission states. Value of luminescence anisotropy factor (g_{lum}=0.0178) calculated by the equation 2(IL-IR)/(IL+IR), which have matched well with quantitative PCD responded from GMG NSs (*g* factor=0.022).[28, 29] IL and IR are the luminescence intensity of GMG NSs functionalized Rodamine B under the irradiation of left-handed and right-handed circularly polarized photons, respectively. In the Figure 3D, well-known Coulomb interaction induces the chiral current inside the metal nanostructures which explains well for the appearance of PCD. Thus, coulomb interactions between the GMG NSs and Rodamine B would lead to asymmetric electron transition inside Rodamine B. Electromagnetic field resulted from the induced chiral current can **destroy the asymmetry ground states/ excited states o**f Rodamine B. The CD band of Cys at 206nm and 261 nm is now strongly coupled with the SPR of metal NPs which induced chiral nanoplasmonics at the visible range. PCD continuously amplified the interference of incident and induced fields of achiral dyes. The first effect comes from enhancement of electric field in the chiral molecule and from Coulomb interaction between a chiral molecule and a nonchiral plasmonic nanostructure. The second effect originates from the giant enhancement of asymmetric electron transition in the energy states of the near dyes via Coulomb interactions.

Conclusions:

To sum it up, we have investigated the controllability of PCD in the discrete GMG NSs. Surface-adsorbed Cys and solution-dispersed Cys not only play the critical role in the morphology control of GMG NSs but also in the PCD enhancement since both kinds of Cys are distributed into the hotspots. Unlike other chiral systems, GMG NSs also give rise many additional unique features. For example, the discrete nanostructures are quite high durability and stability in the tough conditions. Interestingly, chiral molecules have imparted their chiroptical properties to non-covalent achiral dyes via chiral plasmon reporters. Symmetric emission states of achiral dyes have been destroyed via exciton-dipole Coulomb interactions in the discrete GMG NSs. Therefore, the CPL of novel hybrid nanostructures offer the glorious future in the chemistry, materials, and physical fields.

Methods & Materials:

Hexadecyltrimethylammonium bromide (CTAB) and hexadecyltrimethylammonium chloride (CTAC), gold(III) chloride hydrate (chemical formula), L/D-cysteine (L/D-Cys), L-ascorbic acid (AA), $AgNO_3$, rodamine B, HCL(37%), and sodium borohydride ($NaBH_4$) were purchased from Sigma-Aldrich used as received.

Synthesis of gold nanorods:

Gold nanorods were prepared by the seed-mediated growth approach. 10 mL solution of 100 mM CTAB containing 250 μL of $HAuCl_4$ (10 mM) was injected 600 μL of 10 mM $NaBH_4$. This made seed solution was placed quietly at room temperature for 2 h. Growth solution was prepared by adding 2 ml of HAuCL4 (10 mM), 75 ul of AgNO3 (10mM), 0.32ml of AA (0.1M), and 0.8ml of HCL (1.0 M) into 40ml of CTAB solution (0.1 M). Then 96 μL of the synthesized seed solution was added to the growth solution, which was placed quietly at room temperature for 6 h. Finally, the as-prepared gold nanorods were centrifuged twice in water (8000 rpm for 20 min) and redispersed in the same volume of 80mM CTAC for next overgrowth process.

Synthesis of GMG NSs:

Single-crystalline GMG NSs were synthesized as following procedures. To fabricate GMG NSs, different concentration of L/D-Cys added in to 4.575ml 40mM CTAC solution containing 0.02 mM HAuCl4 and 0.01M ascorbic acid (AA). As-synthesized Au NRs were added and gently shake for several seconds. Incubate for 90min to allow for the sys take the new Au nanoseeds generated by AA to surface of gold nanorods through thiol-Au chemical bond. Then, 100ul 10mM Au precursor HAuCl4 was added. After two hours, the produced GMG NSs was washed twice, collected via centrifugation and finally stored into 5 ml water solution.

Conjugation of dye to GMG NSs

10 ml 10^{-2} M rodamine B was added respectively into two vials of 1 ml GMG NSs fabricated in the presence of 20 ul 10^{-5} M L/D Cys and incubated overnight, Samples are stored into 500 ul water solution after centrifugation for CD and PL measurements

Spectroscopic Measurements.

Optical characterization was conducted using an Agilent 8453 UV–visible spectrometer.

All CD spectra were measured by using a commercially available spectropolarimeter (JASCO, J-810) for the L-GMG NSs and D-GMG NSs samples solution in a cuvette. The optical path of sample cells is 10 mm for recoding CD spectra.
The Raman spectra of samples solution was collected through a Leica microscope equipped with a confocal Raman spectroscopic system (Renishaw InVia) and a 785 nm laser excitation source.

The photoluminescence spectra of samples are measured by the Horiba Raman equipped with 1/4 waveplate under irradiation of 488nm laser.

Nanostructure Characterizations.

Conventional TEM images were acquired with a J**EOL JEM 1010** microscope operated at 100 kV. HRTEM characterization is conducted by a transmission electron microscope **(JEM-2010)** operated at ??? kV.

REFERENCES

1. Guerrero-Martinez, A., M. Grzelczak, and L.M. Liz-Marzan, *Molecular Thinking for Nanoplasmonic Design.* Acs Nano, 2012. **6**(5): p. 3655-3662.
2. Guerrero-Martinez, A., et al., *From individual to collective chirality in metal nanoparticles.* Nano Today, 2011. **6**(4): p. 381-400.
3. Zheng, H., et al., *Uncovering the Circular Polarization Potential of Chiral Photonic Cellulose Films for Photonic Applications.* Adv Mater, 2018.
4. Kim, Y., et al., *Reconfigurable chiroptical nanocomposites with chirality transfer from the macro- to the nanoscale.* Nat Mater, 2016. **15**(4): p. 461-8.
5. Zhao, Y., et al., *Shell-Engineered Chiroplasmonic Assemblies of Nanoparticles for Zeptomolar DNA Detection.* Nano Letters, 2014. **14**(7): p. 3908-3913.
6. Lieberman, I., et al., *Plasmon-resonance-enhanced absorption and circular dichroism.* Angewandte Chemie-International Edition, 2008. **47**(26): p. 4855-4857.
7. George, J. and K.G. Thomas, *Surface Plasmon Coupled Circular Dichroism of Au Nanoparticles on Peptide Nanotubes.* Journal of the American Chemical Society, 2010. **132**(8): p. 2502-+.
8. Ben Moshe, A., D. Szwarcman, and G. Markovich, *Size Dependence of Chiroptical Activity in Colloidal Quantum Dots.* Acs Nano, 2011. **5**(11): p. 9034-9043.
9. Han, B., et al., *Conformation Modulated Optical Activity Enhancement in Chiral Cysteine and Au Nanorod Assemblies.* Journal of the American Chemical Society, 2014. **136**(46): p. 16104-16107.
10. Fan, Z.Y. and A.O. Govorov, *Plasmonic Circular Dichroism of Chiral Metal Nanoparticle Assemblies.* Nano Letters, 2010. **10**(7): p. 2580-2587.
11. Govorov, A.O., et al., *Theory of Circular Dichroism of Nanomaterials Comprising Chiral Molecules and Nanocrystals: Plasmon Enhancement, Dipole Interactions, and Dielectric Effects.* Nano Letters, 2010. **10**(4): p. 1374-1382.
12. Wu, X.L., et al., *Gold Core-DNA-Silver Shell Nanoparticles with Intense Plasmonic Chiroptical Activities.* Advanced Functional Materials, 2015. **25**(6): p. 850-854.
13. Hao, C.L., et al., *Unusual Circularly Polarized Photocatalytic Activity in Nanogapped Gold-Silver Chiroplasmonic Nanostructures.* Advanced Functional Materials, 2015. **25**(36): p. 5816-5822.
14. Kou, X.S., et al., *Glutathione- and cysteine-induced transverse overgrowth on gold nanorods.* Journal of the American Chemical Society, 2007. **129**(20): p. 6402-+.
15. Pour, S.O., et al., *Through-space transfer of chiral information mediated by a plasmonic nanomaterial.* Nature Chemistry, 2015. **7**(7): p. 591-596.
16. Morrow, S.M., A.J. Bissette, and S.P. Fletcher, *Transmission of chirality through space and across length scales.* Nature Nanotechnology, 2017. **12**(5): p. 410-419.
17. Zhu, Z.N., et al., *Controllable Optical Activity of Gold Nanorod and Chiral Quantum Dot Assemblies.* Angewandte Chemie-International Edition, 2013. **52**(51): p. 13571-13575.
18. de Aberasturi, D.J., et al., *Surface Enhanced Raman Scattering Encoded Gold Nanostars for Multiplexed Cell Discrimination.* Chemistry of Materials, 2016. **28**(18): p. 6779-6790.
19. Lim, B. and Y.N. Xia, *Metal Nanocrystals with Highly Branched Morphologies.* Angewandte Chemie-International Edition, 2011. **50**(1): p. 76-85.
20. Coronado-Puchau, M., et al., *Enzymatic modulation of gold nanorod growth and application to nerve gas detection.* Nano Today, 2013. **8**(5): p. 461-468.
21. Zhang, L., et al., *Synthesis of Convex Hexoctahedral Palladium@Gold Core-Shell Nanocrystals with {431} High-Index Facets with Remarkable Electrochemiluminescence Activities.* ACS Nano, 2014. **8**(6): p. 5953-5958.
22. Lee, H.E., et al., *Concave Rhombic Dodecahedral Au Nanocatalyst with Multiple High-Index Facets for CO2 Reduction.* ACS Nano, 2015. **9**(8): p. 8384-8393.
23. Zhang, H. and A.O. Govorov, *Giant circular dichroism of a molecule in a region of strong plasmon resonances between two neighboring gold nanocrystals.* Physical Review B, 2013. **87**(7).
24. Feng, Y.H., et al., *An Unconventional Role of Ligand in Continuously Tuning of Metal-Metal Interfacial Strain.* Journal of the American Chemical Society, 2012. **134**(4): p. 2004-2007.
25. Wang, R.Y., et al., *Experimental Observation of Giant Chiroptical Amplification of Small Chiral Molecules by Gold Nanosphere Clusters.* Journal of Physical Chemistry C, 2014. **118**(18): p. 9690-9695.
26. Yang, D., et al., *Chirality and energy transfer amplified circularly polarized luminescence in composite nanohelix.* Nature Communications, 2017. **8**.
27. Kumar, J., T. Kawai, and T. Nakashima, *Circularly polarized luminescence in chiral silver nanoclusters.* Chemical Communications, 2017. **53**(7): p. 1269-1272.
28. Yan, J.L., et al., *Chiroptical Resolution and Thermal Switching of Chirality in Conjugated Polymer Luminescence via Selective Reflection using a Double-Layered Cell of Chiral Nematic Liquid Crystal.* Advanced Functional Materials, 2017. **27**(2).
29. Chen, S.H., et al., *Circularly polarized light generated by photoexcitation of luminophores in glassy liquid-crystal films.* Nature, 1999. **397**(6719): p. 506-508.